Lighting estimation in fringe images during motion compensation for 3D measurements

Andreas Breitbarth[a], Peter Kühmstedt[a], Gunther Notni[a] and Joachim Denzler[b]

[a]Fraunhofer IOF, Albert-Einstein-Str. 7, 07745 Jena, Germany;
[b]Friedrich Schiller University Jena, Chair for Computer Vision, Ernst-Abbe-Platz 2, 07743 Jena, Germany

ABSTRACT

Fringe projection is an established method to measure the 3D structure of macroscopic objects. To achieve both a high accuracy and robustness a certain number of images with pairwise different projection pattern is required. Over this sequence it is necessary that each 3D object point corresponds to the same image point at every time. This situation is no longer given for measurements under motion. One possibility to solve this problem is to restore the static situation. Therefore, the acquired camera images have to be realigned and secondly, the degree of fringe shift has to be estimated. Furthermore, there exists another variable: change in lighting. The compensation of these variances is a difficult task and could only be realized with several assumptions, but it has to be approximately determined and integrated into the 3D reconstruction process.

We propose a method to estimate these lighting changes for each camera pixel with respect to their neighbors at each point in time. The algorithms were validated on simulation data, in particular with rotating measurement objects. For translational motion, lighting changes have no severe effect in our applications. Taken together, without using high-speed hardware our method results in a motion compensated dense 3D point cloud which is eligible for three-dimensional measurement of moving objects or setups with sensor systems in motion.

Keywords: 3D measurements, fringe projection, moving objects motion compensation, lighting changes

1. INTRODUCTION

Optical 3D measurement with an active projection of a couple of pairwise different pattern is a well establish approach in the area of quality control and rapid prototyping.[1] However, dealing with moving measurement objects or non-static 3D sensors, e.g. handheld systems[2], is a challenging task, due to variable point correspondences between the cameras and variable correlations between 2D camera points and 3D object points. Basically all methods that work in static situations require pixelwise correspondences over the process of 3D measurement. Correspondences are thereby defined as a fixed triple of one 2D point in each camera plane - the points for later triangulation[3] - and the 3D object point, that is projected to the two mentioned 2D points. Working only with one camera and one projector the triple consists of the 3D object point, one 2D point in the camera plane and one 3D point in the projector plane.

For relative motion these triples are no longer fixed over the whole measurement process. As relative motion we define motion between the sensor system and the measurement object. If both moved in the same way, e.g. a production line and a flying sensor with the same direction and velocity, the value for relative motion is zero and the measurement setup can be assumed as static. For setups with a relative motion diverse to zero several methods have been developed in the last years, e.g. a two-step phase shift algorithm in Yang and He[4], an approach of combining several patterns in Guan et al.[5] and a so called stripe boundary pattern projection[6,7]. Most of

these approaches deal with high-speed hardware or a minor number of projection pattern resulting in very short cycle time for pattern projection and image aquisition, so that the motion or value changes for the mentioned point triple could be assumed as approximately zero. Due to the fact that most digital projection systems did not work faster than 60 Hz, the high-speed approach has several limitations. For phase shifting algorithms at least three different pattern are required. These three patterns can be integrated into one projection cycle. Therefore, each pattern is dedicated to each of the three color channels. For higher measurement accuracy, especially on colored measurement objects, it is recommended to eliminate the color filters on the color wheel and work with gray scale cameras and images, as e.g. described in Zhang and Huang,[8] Huang et al.[9] and Huang et al.[10].

Another possibility to handle relative motion during 3D measurements is the use of color codings. As described in Salvi et al.,[11] Adán et al.,[12] Albitar et al.[13] and many other publications, stripes or so called M-array-point distributions are used to mark 3D object points for a better search of 2D point correspondences relating to the 3D object points. For uniqueness of each marker the colors of points or stripes in a pre-defined neighborhood are choosen in a special, so called "disordered" way. Salvi et al. use six basic colors to encode rows and columns of the projected stripes. High details are achieved by Adán et al. using a point coding with seven different symbols respectively colors in a hexagonal arrangement. Concerning an irrelevant collocation of these color points in one neighborhood, theoretically 6468 different code words are possible. All publications with the basic approach of color coding points or stripes exploit the common fact: There is need of only one coding pattern, although the detailedness and possible measurement accuracy is even low.

In 2008, König and Gumhold[14] described an advanced phase-shifting technique for optical 3D reconstruction which deals with slow and timewise linear object motion. These authors extended the known sequence of fringe pattern by bright and dark images and special pattern for tracking respectively 3D motion estimation. Bright and dark images mean that the projection unit projects a unique homogeneous white pattern for the bright image and a homogeneous black pattern (projection unit off) for the dark image. To track the measurement object and to estimate the motion, a special tracking pattern is projected on the surface of the 3D object. Best results are achieved with perlin noise[15] as texture of the tracking pattern.

A similar approach to measure 3D data of moving objects by using fringe projection is described in Breitbarth et al.[16] Thereby we also used two major steps to rebuild an approximately static measurement setup: First, a step of motion estimation in 3D, and second, a step of motion compensation. To estimate the 3D motion between two sequently images, coarse 3D data have to be obtained. This is done by fourier analysis of each of the aquired fringe images.[17] Of course, the use of fourier transform only yields in coarse 3D point clouds. But this intermediate results are sufficient to estimate the motion approximately between two sequently fringe images each in 3D space. For motion estimation, algorithms of iterative point clouds (ICP[18]) are used. The

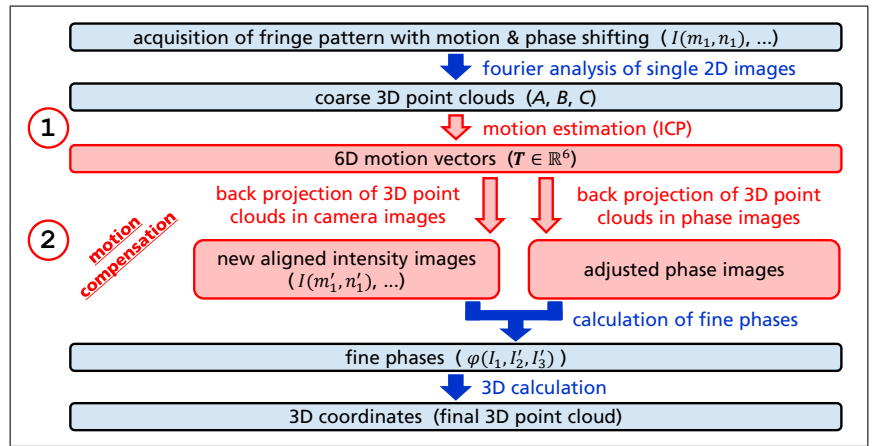

Figure 1. Flow chart of major steps for 3D measurements with relative motion, with the aquisition of fringe pattern at the beginning and resulting in a dense 3D point cloud. With blue background the well known steps from phase shifting techniques with fringe projection, red highlighted the additional parts of motion estimation ① and compensation ②.

effect of motion errors to final 3D point clouds with motion compensated fringe images and phase shift values is also described in Breitbarth et al. (2012). Figure 1 shows a flow chart of the major steps that have to be done in general for motion compensation for 3D measurements with active fringe projection.

Our mentioned publication from 2012[16] has one major disadvantage: It only works for translational motion, in which changes in lighting could be assumed as approximately zero for a sensor system. This is accomplished by orthographic projection on convex object surfaces. For concave surfaces or especially arbitrary rotations of the measurement object, lighting changes have to be taken into account, which is done in this publication and theoretically described in the following section.

2. MATHEMATICAL APPROACH OF LIGHTING ESTIMATION

The well known equation to describe intensity distributions during phase sampling evaluation

$$I_n(x,y) = a(x,y) + b(x,y) \cdot \cos[\phi(x,y) + \Delta\phi_{R_n}]$$ (1)

consists of three unknowns (the additive and multiplicative intensity distortions $a(x,y)$ and $b(x,y)$, and the phase distribution $\phi(x,y)$). Thus, there is need for at least three pairwise different fringe pattern. The solution of the nonlinear system by gaussian least squares approach with $u(x,y) = b(x,y) \cdot cos[\phi(x,y)]$ and $v(x,y) = b(x,y) \cdot sin[\phi(x,y)]$, rewritten as sum of quadratic errors yields in

$$\begin{pmatrix} m & \sum \cos \Delta\phi_{R_n} & \sum \sin \Delta\phi_{R_n} \\ \sum \cos \Delta\phi_{R_n} & \sum \cos^2 \Delta\phi_{R_n} & \sum \cos \Delta\phi_{R_n} \cdot \cos \Delta\phi_{R_n} \\ \sum \sin \Delta\phi_{R_n} & \sum \cos \Delta\phi_{R_n} \cdot \cos \Delta\phi_{R_n} & \sum \sin^2 \Delta\phi_{R_n} \end{pmatrix} \cdot \begin{pmatrix} a \\ u \\ v \end{pmatrix} = \begin{pmatrix} \sum I_n \\ \sum I_n \cdot \cos \Delta\phi_{R_n} \\ \sum I_n \cdot \sin \Delta\phi_{R_n} \end{pmatrix}$$ (2)

For static measurement setups the intensity distortions can be assumed as constants, so phase distributions $\phi(x,y)$ are calculated with respect to intensity images and values of phase shifting. As described in the introduction and shown in figure 2 lighting parameters are no longer constant for measurement setups with relative motion. So the additive and multiplicative intensity distortions $a(x,y)$ and $b(x,y)$ have to be taken into account. This could be done using the equation system (2). Two major differences have to be mentioned for the dynamic setup, i.e. the situation with relative motion unequal to zero:

1. Phase shifting between two images or time steps is no longer unique in global area, depending on the 3D structure and surface of the measurement object each pixel has a different phase shifting value $\Delta\phi_{R_n}(x,y)$.

2. Intensity values are taken from motion compensated respectively realigned fringe images $\widehat{I}^c_n(x,y)$. The index c describes the camera number.

These adaptations lead to an equation system similar to the system (2):

$$\begin{pmatrix} m_{nh} & \sum \cos \Delta\phi_{R_n}(x,y) & \sum \sin \Delta\phi_{R_n}(x,y) \\ \sum \cos \Delta\phi_{R_n}(x,y) & \sum \cos^2 \Delta\phi_{R_n}(x,y) & \sum \cos \Delta\phi_{R_n}(x,y) \cdot \cos \Delta\phi_{R_n}(x,y) \\ \sum \sin \Delta\phi_{R_n}(x,y) & \sum \cos \Delta\phi_{R_n}(x,y) \cdot \cos \Delta\phi_{R_n}(x,y) & \sum \sin^2 \Delta\phi_{R_n}(x,y) \end{pmatrix} \cdot \begin{pmatrix} a^c_n(x,y) \\ u^c_n(x,y) \\ v^c_n(x,y) \end{pmatrix}$$
$$= \begin{pmatrix} \sum \widehat{I}^c_n(x,y) \\ \sum \widehat{I}^c_n(x,y) \cdot \cos \Delta\phi_{R_n}(x,y) \\ \sum \widehat{I}^c_n(x,y) \cdot \sin \Delta\phi_{R_n}(x,y) \end{pmatrix}$$ (3)

While additive intensity distortion $a^c_n(x,y)$ is yield directly, the multiplicative intensity distribution respectively the parameter for local fringe contrast $b^c_n(x,y)$ have to be calculated with the next equation:

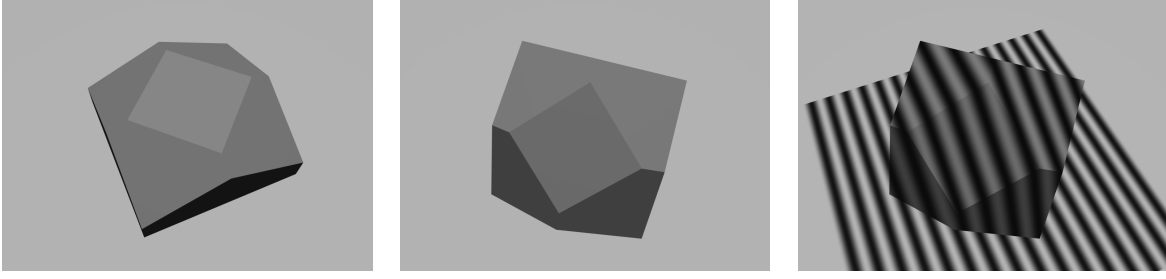$$b^c_n(x,y) = \sqrt{[u^c_n(x,y)]^2 + [v^c_n(x,y)]^2}$$ (4)

Figure 2. Example for lighting changes during a rotating prism around the x and z axis. Left the first image of the measurement sequence, the two other images are aquired at time step 21 - in the middle without any projection, right with a sinusoidal intensity distribution.

Remember that m in (2) is defined as the number of used images, there exists a trade-off in the case of optical 3D measuring with relative motion:

$$m \stackrel{def}{=} \text{number of images} \quad vs. \quad \text{lighting values necessary for } each \text{ moment in time/image } n.$$

So we assumed that there are no significant changes in lighting values between adjacent pixels and solve the equation system (3) for each pixel (x, y) in every single fringe image n with respect to values $\Delta\phi_{R_n}(x, y)$ and $\widehat{I}_n^c(x, y)$ in a spatial neighborhood m_{nh}. How we define the neighborhood is specified later.

To calculate the phase distribution $\phi(x, y)$ for each camera and each projection direction we use a generic solution for 3D measurements with variable phase steps, publicated by Farell and Player in 1992.[19] To apply this method directly is not possible since we have nonhomogeneous phase step values in global. Further, the estimation of lighting parameters by using the mentioned ellipse fitting method is not feasible. But with the previous steps of motion compensation (especially the estimation of local phase shifting values $\Delta\phi_{R_n}(x, y)$) and the equations (3) and (4) described in detail, we could calculate phase values with an advanced generic solution. Phase distribution $\phi(x, y)$ is calculated by the following equations:

$$\phi^c(x, y) = \arctan \frac{\left[\sum_n b_n^c(x, y) \cos^2 \Delta\phi_{R_n}(x, y)\right] \cdot S(x, y) - \left[\sum_n b_n^c(x, y) \sin \Delta\phi_{R_n}(x, y) \cos \Delta\phi_{R_n}(x, y)\right] \cdot C(x, y)}{\left[\sum_n b_n^c(x, y) \sin \Delta\phi_{R_n}(x, y) \cos \Delta\phi_{R_n}(x, y)\right] \cdot S(x, y) - \left[\sum_n b_n^c(x, y) \sin^2 \Delta\phi_{R_n}(x, y)\right] \cdot C(x, y)}$$

(5)

with

$$C = \sum_n \left[\widehat{I}_n^c(x, y) \cdot \cos \Delta\phi_{R_n} - a_n^c \cdot \cos \Delta\phi_{R_n}\right] \quad \text{and} \quad S = \sum_n \left[\widehat{I}_n^c(x, y) \cdot \sin \Delta\phi_{R_n} - a_n^c \cdot \sin \Delta\phi_{R_n}\right].$$

3. TRIVIAL TEST AND FURTHER ADDITIONS

To verify our proposed algorithms we execute a fundamental mesaurement setup. Therefore, we simulate four images. Each of them consists of eight sinusoidal curves as intensity distribution. Of course, we integrate a global phase shifting of $\Delta\phi_{R_n} = 90°$ between two successive fringe images. Phase sampling evaluation with the approach for static measurement setups works fine, so we can take the same four images as input for our new method. For the intensity distortion maps a and b we receive the values zero respectivly one as expected. The final fine phase maps looks also good and as 3D result we obtained a perfect plain.

We continued and simulated four fringe images with a light fall off beginning at the image center. One of the used images is seen in figure 3 on the left hand side. Phase sampling evalution without lighting changes are taken into account yields in wrong fine phase distributions as plotted in figure 3 in the middle. The failure is reflected in the non periodicity of the 2π-wrapped fine phases. Figure 3 shows on the right hand side the correct result which is obtained by our proposed algorithms including pixelwise lighting estimation.

Next step in the process of evaluation is the measurement of an 3D object which was simulated firstly. We decide to use a convex object and take a prism. Remember, three different $\left(\widehat{I}_n^c(x, y), \Delta\phi_{R_n}(x, y)\right)$ tuple are enough to solve the equation system (3), so we take the four diagonal adjacent pixels for each image position (x, y)
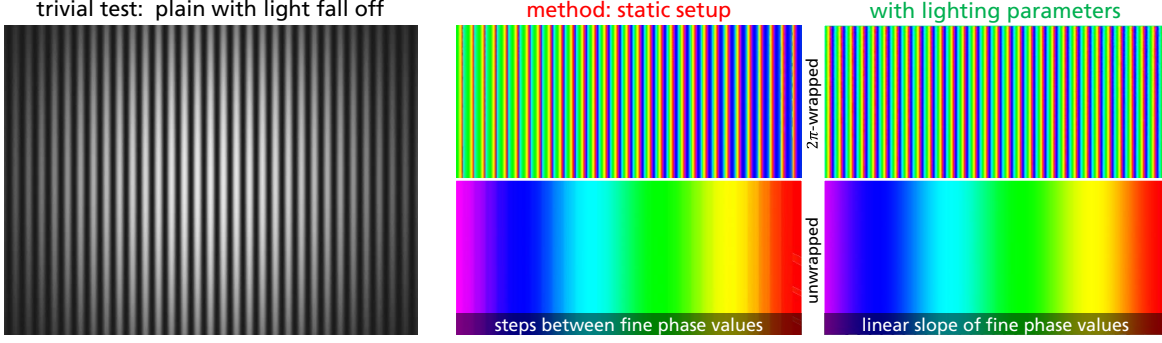
Figure 3. Basic verification of proposed algorithms. On the left hand side one fringe image with light fall off beginning at the image center. Fine phase maps without consideration of lighting changes in the middle and results with the new algorithms on the right hand side. Fine phase maps at the top shows the 2π-wrapped states, the unwrapping results are shown at the bottom.

into account. The resulting fine phase maps look partly very noisy. Thus, we increase the size of neighborhood and the number of input tuple m_{nh}. Depending on the projection direction p_{dir} we use adjacent pixel values out of the diagonals (p_{dir} approximatly parallel to image axis) or parallel to the image axes. Figure 4 shows the 2π-wrapped fine phase results with a kernel size of seven pixel on the left and a kernel size of 31 pixel on the right hand side. The images point out, that the proposed algorithms basically estimate correct finephases. But there are two problems left:

- For minor kernel sizes we obtain partwise noisy results, especially at regions with low contrast (values of $b(x, y)$ smaller than 0.5) and image parts with wide fringe periods.

- On the other side major kernel sizes yields in very smooth fine phase distributions which are undesirably at edges of the 3D mesurement object.

The solution could be an adaptive choice of kernel sizes only. Because sinus and cosinus functions has no linear slope, the decision of kernel size can not based on gray value gradients in the fringe images. But we can still use the estimated phase shift distribution and calculate gradients based on these images. This is represented in the steps of algorithm 1 for lighting estimation.

The returned lighting distributions a_n^c and b_n^c in combination with the motion compensated fringe images $\widehat{I}_n^c$ are taken as input for equation (5) and results in 2π-wrapped fine phase maps ϕ^c. The process of unwrapping based on the back projection in projector plain, where each fringe period is determined. The triangulation for estimating final 3D point clouds is realized in the same way as performed for static measurement setups.
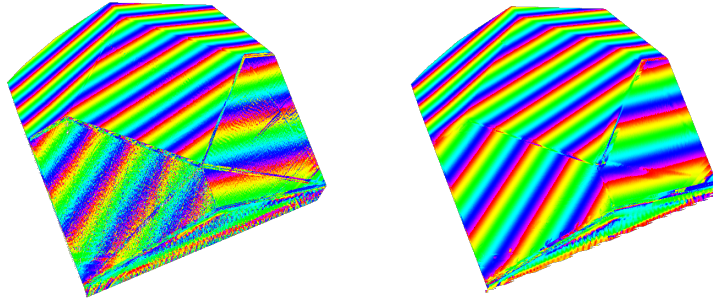

Figure 4. Influence of the kernel size to the fine phase maps in the process of lighting estimation. For the left result a kernel size of seven pixel is used, that means that three adjacent pixel in each direction are taken into account starting at the actual position (x, y). Results with a greater kernel size of 31 pixel are shown on the right hand side. In this case there is no noise at planar object parts but smoothness at edges are to high.

Algorithm 1: Lighting estimation during motion compensation

    Data: motion compensated fringe images $\widehat{I}_n^c$, local phase shifting $\Delta\phi_{R_n}$

    Result: lighting distributions a_n^c and b_n^c

    for c=1:cam **do**

        for n=1:image/point in time **do**

            for (x,y)=(1,1):(width,height) **do**

                reference phase values $\Delta\phi_{R_n}^c(x,y)$ back projected in camera plane

                estimate gradients $\nabla(x,y)$ with 3×3 sobel operator on $\Delta\phi_{R_n}^c$ maps

                for 4 directions (2 along axis *and* 2 diagonals) **do**

                    seach max $\Delta\left[\Delta\phi_{R_n}^c(x,y)\right]$ ($\equiv$ orthogonal to projection direction)

                end

                for 2 directions (2 along axis *or* 2 diagonals, start at (x,y)) **do**

                    search $\max\limits_{(x',y')} dist[(x,y)-(x',y')]$ with $\Delta\phi_{R_n}$ thresholds

                end

                solve equation system (2)* with max. number of input values

                calculate $b_n^c(x,y)$ out of 2nd and 3rd entry in result vector of previous step

            end

        end

    end

---

4. EXPERIMENTS AND RESULTS

In the previous section, we showed the basic operability of the proposed algorithms for 3D measurement with lighting changes. Nevertheless, some problems dealing with edges of the measurement objects and regions with low contrast of fringe projection are still remaining. To resolve this issues we modify our approach and use an algorithm with an adaptive kernel size for estimating the lighting parameters as it is shown in algorithm 1. To validate these modifications we execute several tests. Since we want to see only the influence of lighting estimation on results of 3D measurement, we used simulations with á priori known 3D object points and known motion vectors as input for the part of motion compensation.

Similar to the first tests we simulate a prism with an edge length of 180 mm. All simulations were done by the raytracing tool POV-Ray version 3.7. For a higher level of reality the simulated object includes shades and we add non homogeneous ambient light. In several applications measurement objects have no colored textures. Thus, we used a shade of gray as pigment. Further, we used the perspective projection for the two cameras and the projection unit. The projection sequence consists of 16 fringe pattern, eigth for each projection direction. So we have an input phase shift of about $\Delta\phi_{R_n} = 45°$ between two sequently fringe images and the projection directions are rotated $90°$ to each other. Due to the back projection process in the projector plain, additional pattern like a bright and dark image and gray code pattern are not necessary.

To evaluate different lighting changes we translate and rotate our prism with all possible combinations of the three axes X, Y and Z. Results of the principal operability, the completeness of the wrapped 3D point clouds with respect to the ground truth model and the average 3D error are shown in table 1. For evaluation of completeness and the average 3D error only parts of the ground truth model that are visible from one point of view are taken into account.

Because the achieved results look very well and there are no obvious limitations, we add some gaussian noise to the input fringe images. Results are plotted in figure 5. There exists a exponential relation between noise level and average 3D error. Remembering the edge length of the measurement object $l_{prism} = 180$ mm and a field of view of $400\,\text{mm} \times 300\,\text{mm}$ an average 3D error greater than $err_{avg}^{3D} = 0.4$ ($\equiv 1/1000 * \text{FoV}$) is not usefull for the most applications. Anyway, the proposed algorithms especially the part of lighting estimation operates quite well for fringe images with major noise. Beginning at a noise level of $RMS = 5$ first fine phase errors can be detected by visual examination.

Table 1. Verification of the proposed algorithms for 3D measurement with lighting changes. For object motion which is marked by a # (symbol * in result rows) some parts of the prism are only temporary viewable, so we yield some errors at period borders that are not founded by our algorithms. The size of used motion between two sequently images is 3 mm for translation and 3 degree for rotation, so in total 21 mm / 21 degree for each projection direction.

object motion	w/o lighting estimation	extended approach		
		visual verification	completeness	avg. 3D error
translation X	✓	✓	99.5 %	36 µm
translation Y	✓	✓	99.5 %	244 µm
translation Z/scaling	✓	✓	99.6 %	35 µm
translation XY	✓	✓	98.0 %	251 µm
translation XZ	◯	✓	99.6 %	38 µm
translation YZ	◯	✓	99.6 %	283 µm
translation XYZ	◯	✓	98.9 %	301 µm
rotation X	◯	✓	99.3 %	208 µm
rotation Y$^{\#}$	◯	✓*	92.3 %*	164 µm
rotation Z	✓	✓	97.6 %	157 µm
rotation XY$^{\#}$	✗	✓*	89.2 %*	274 µm
rotation XZ	✗	✓	99.0 %	164 µm
rotation YZ$^{\#}$	✗	✓*	85.8 %*	163 µm
rotation XYZ	✗	✓	98.9 %	171 µm

For one further experiment we add some objects to our simulation scene, which create huge shades on parts of our prism. These shadowed regions are not completely black, so that theoretically phase sampling evaluation and calculation of 3D points are possible. Figure 6 shows one of the input fringe images on the left hand side. The fine phase map $\phi(x, y)$ in the middle of figure 6 is the result of phase sampling evaluation without shades introduced by other objects than the measurement object as reference; the results with shadowed regions in input images are shown on the right. Most parts of the object are reconstructed correctly. All errors of fine phase values are located at the region near to the border of shades. These regions detected as object edges by the mentioned algorithm 1, the used kernel sizes and number of used values as input in equation system (3) are not that high. To circumvent this issue, further investigations are required.
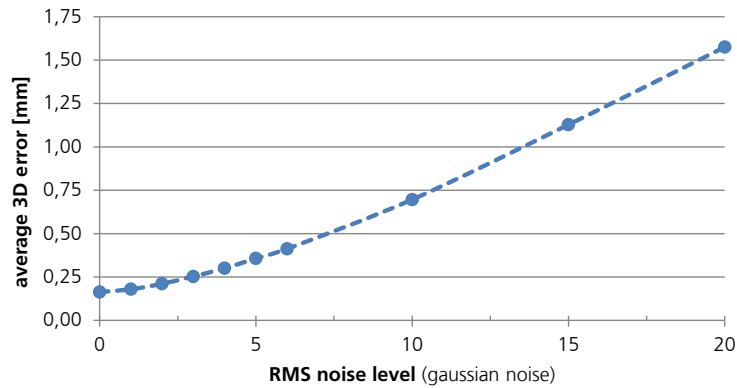

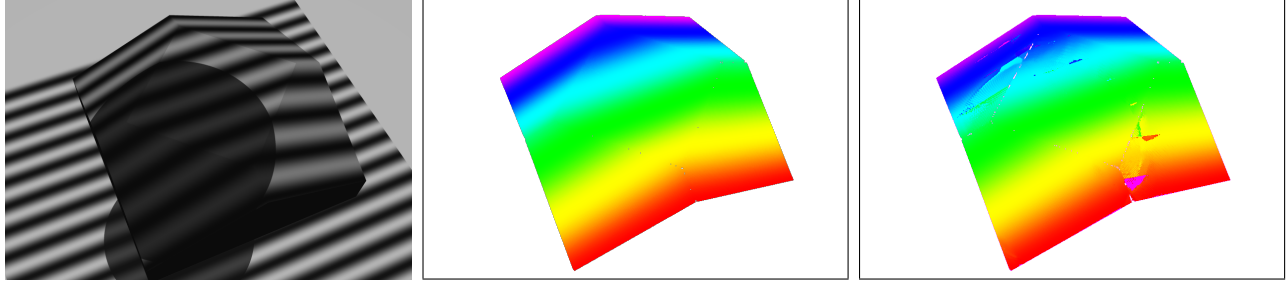Figure 5. Influence of gaussian noise to 3D results.

Figure 6. 3D measurement of moved objects with shades introduced by other objects. Left: First image of the sequence of fringe pattern. 2π unwrapped fine phases without the influence of shades in the middle and an erroneous fine phase map at the right as result out off fringe images with shadowed regions.

To conclude our verifications we accomplish one experiment with real input data. Similar to the explained simulations we take full 3D data and known object motion as input into the process of motion compensation with lighting estimation. The full 3D data were obtained out of a previous 3D measurement with static setup. The measurement object is a prism, too. Achieved results point out that there is no significant difference between simulation and real data.

5. CONCLUSION

We have presented a new approach for 3D measurement of macroscopic objects including relative motion under the process of pattern projection and image aquistion. In contrast to our publication in 2012[16] our proposed algorithms operates on rotating objects, too. Experiments with several level of noise and shades introduced by other objects verify the additional steps of lighting estimation in the overall process of motion compensation. Only borders of shades are still a challenging task and should be part of further research.

In addition, reducing calculation time would be a nice feature for further experiments. Currently the part of lighting estimation need approximately one minute at one $2.8\,\mathrm{GHz}$ core of a PC with a i7 first generation CPU. All other parts of motion compensation need less than ten seconds in total.

REFERENCES

[1] Schreiber, W. and Notni, G., "Theory and arrangements of self-calibrating whole-body three-dimensional measurement systems using fringe projection technique," *Optical Engineering* **39**, 159–169 (2000).

[2] Munkelt, C., Schmidt, I., Brauer-Burchardt, C., Kuehmstedt, P., and Notni, G., "Cordless portable multi-view fringe projection system for 3d reconstruction," in [*Computer Vision and Pattern Recognition*], (2007).

[3] Luhmann, T., Robson, S., Kyle, S., and Harley, I., [*Close Range Photogrammetry*], Whittles Publishing (2006).

[4] Yang, F. and He, X., "Two-step phase-shifting fringe projection profilometry: intensity derivative approach," *Applied Optics* **46**, 7172–7178 (2007).

[5] Guan, C., Hassebrook, L. G., and Lau, D. L., "Composite structured light pattern for three-dimensional video," *Optics Express* **11**, 406–417 (March 2003).

[6] Hall-Holt, O. A. and Rusinkiewicz, S., "Stripe Boundary Codes for Real-Time Structured-Light Range Scanning of Moving Objects," in [*International Conference on Computer Vision*], 359–366 (July 2001).

[7] Rusinkiewicz, S., Hall-Holt, O., and Levoy, M., "Real-Time 3D Model Acquisition," *ACM Transactions on Graphics* **21**, 438–446 (July 2002).

[8] Zhang, S. and Huang, P. S., "High-resolution, real-time three-dimensional shape measurement," *Optical Engineering* **45**, 123601 (December 2006).

[9] Huang, P. S., Hu, Q., Jin, F., and Chiang, F.-P., "Color-encoded digital fringe projection technique for high-speed three-dimensional surface contouring," *Optical Engineering* **38**(6), 1065–1071 (1999).

[10] Huang, P. S., Zhang, C. P., and Chiang, F. P., "High-speed 3-D shape measurement based on digital fringe projection," *Optical Engineering* **42**(1), 163–168 (2003).

[11] Salvi, J., Batlle, J., and Mouaddib, E. M., "A robust-coded pattern projection for dynamic 3d scene measurement.," *Pattern Recognition Letters* **19**(11), 1055–1065 (1998).

[12] Adán, A., Molina, F., and Morena, L., "Disordered patterns projection for 3d motion recovering.," in [*3DPVT*], 262–269, IEEE Computer Society (2004).

[13] Albitar, C., Graebling, P., and Doignon, C., "Robust structured light coding for 3d reconstruction.," in [*ICCV*], 1–6, IEEE (2007).

[14] König, S. and Gumhold, S., "Image-based motion compensation for structured light scanning of dynamic surfaces.," *IJISTA* **5**(3/4), 434–441 (2008).

[15] Perlin, K., "Improving noise," in [*Computer Graphics*], **35**(3) (2001).

[16] Breitbarth, A., Kühmstedt, P., Notni, G., and Denzler, J., "Motion compensation for three-dimensional measurements of macroscopic objects using fringe projection," in [*DGaO Proceedings*], **113** (2012).

[17] Takeda, M. and Mutoh, K., "Fourier transform profilometry for the automatic measurement of 3-D object shapes," *Applied Optics* **22**(24), 3977–3982 (1983).

[18] Rusinkiewicz, S. and Levoy, M., "Efficient variants of the ICP algorithm," in [*Third International Conference on 3D Digital Imaging and Modeling (3DIM)*], (June 2001).

[19] Farrell, C. T. and Player, M. A., "Phase step measurement and variable step algorithms in phase-shifting interferometry," *Measurement Science and Technology* **3**(10), 953–958 (1992).